Paleoceanography and Paleoclimatology

RESEARCH ARTICLE
10.1029/2020PA003909

Special Section:
The Miocene: The Future of the Past

Persistent Provenance of South Asian Monsoon-Induced Silicate Weathering Over the Past 27 Million Years

Sajid Ali[1,2], Ed C. Hathorne[1], and Martin Frank[1]

[1]Paleoceanography, GEOMAR Helmholtz Centre for Ocean Research Kiel, Kiel, Germany, [2]Birbal Sahni Institute of Palaeosciences (BSIP), Lucknow, India

Key Points:

- Relatively stable mixture of source rocks weathered to clays over the past 27 Myrs
- Pronounced increase in primary clay minerals occurred 13.9 Myrs ago
- Shift in weathering regime possibly result of winter monsoon dry season development

Supporting Information:

- Supporting Information S1
- Data Set S1
- Data Set S2
- Data Set S3
- Data Set S4

Correspondence to:
S. Ali and E. C. Hathorne,
sajidali@bsip.res.in;
ehathorne@geomar.de

Citation:
Ali, S., Hathorne, E. C., & Frank, M. (2021). Persistent provenance of South Asian monsoon-induced silicate weathering over the past 27 million years. *Paleoceanography and Paleoclimatology*, *36*, e2020PA003909. https://doi.org/10.1029/2020PA003909

Received 7 MAR 2020
Accepted 12 FEB 2021

Abstract The development of the South Asian monsoon (SAM) and Himalaya-Tibetan Plateau uplift were closely intertwined with some studies suggesting that uplift initiated the monsoon whereas others link tectonics with monsoon-controlled exhumation. Silicate weathering controls atmospheric CO_2 on geological timescales resulting in a large potential for monsoon strength and the Himalayan orogeny to influence global climate but detailed records of SAM-induced weathering on million year (Myr) timescales are lacking. Here, we present radiogenic Sr, Nd, and Pb isotope compositions of clay minerals produced by silicate weathering and transported to the central Bay of Bengal. The radiogenic isotope data exhibit a relatively small range and demonstrate a remarkably consistent mixture of sources dominated by Himalayan rocks and the Indo-Burman ranges, which consist of sediments derived from the Himalayas. This suggests that the spatial pattern of regional weathering, which today is highest in the regions of strongest monsoon rains, has persisted in a similar form for the last 27 Myrs. A pronounced increase in primary clay mineral abundance (from 9% to 22%) coincident with global cooling 13.9 Myrs ago points to a shift in the weathering regime given that the clay provenance did not change dramatically. Relatively weaker chemical weathering intensity during the mid and late Miocene cooling suggests increased aridity and changes in the large scale atmospheric circulation in the SAM domain. The establishment of the dry winter monsoon season during the mid and late Miocene may have caused this shift in the weathering regime and can reconcile much of the contrasting evidence for SAM initiation.

1. Introduction

The collision of India with the Eurasian plate and the subsequent uplift of the Himalayas and Tibetan Plateau (HTP) have been implicated in the development of the Asian monsoon system (Molnar et al., 1993) and the consequent increased drawdown of atmospheric CO_2 through enhanced silicate weathering or organic carbon burial (France-Lanord & Derry, 1997; Raymo & Ruddiman, 1992). A reduction of atmospheric CO_2 associated with HTP uplift has been invoked as a cause of major global cooling and establishment of permanent Antarctic ice sheets that characterized the transition from the Cenozoic greenhouse to the present icehouse climate (Raymo & Ruddiman, 1992). The development of the monsoon has even been suggested to have itself influenced HTP tectonics by increased erosion and exhumation (e.g., Clift et al., 2008; Harris, 2007; Iaffaldano et al., 2011). The timing of Asian monsoon development is debated with proposed ages clustering around the Late Miocene (~8–11 Myrs ago) (Molnar et al., 1993) and Late Oligocene/Early Miocene (~25–22 Myrs ago) (Clift et al., 2008; Guo, 2002) but there is even evidence for a strong seasonality of precipitation in the region as early as ~39 Myrs ago (Licht et al., 2014). The elevation histories of the Himalayas and the Tibetan Plateau are poorly constrained and most likely distinct with data suggesting significant elevation of parts of Tibet prior to collision with India and a well-developed proto-plateau by the Eocene (see review by Wang et al., 2014). There are even fewer paleo-elevation data for the Himalayas with recent studies suggesting that the mountains just south of the Yarlung-Tsangpo suture were higher than 2 km in the early Miocene and at a similar elevation to today for at least the past 15 Myrs (Ding et al., 2017; Gébelin et al., 2013). The uplift and exhumation histories of different regions within the Himalayas were also likely asynchronous with the age of exposed leucogranites decreasing from west to east along the central Himalaya (Harris, 2007; Webb et al., 2017). The orographic insulation caused by the Himalayas is thought to have been an important driver of monsoon evolution (Boos & Kuang, 2010) but our understanding of the interaction of tectonics, monsoon-driven erosion, silicate weathering and global

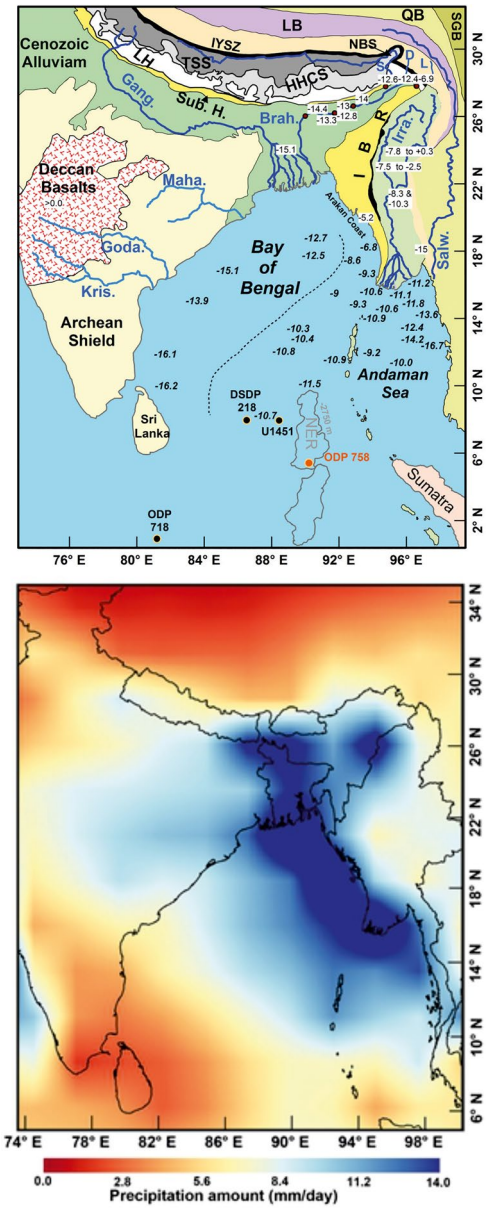

Figure 1. (a) Geological map of source regions of the Bay of Bengal sediments. The location of the ODP Site 758 on the Ninety East Ridge (NER) and other drill core sites discussed are marked. Nd isotope data of river sediments and marine sediments are shown in italics (sources and details in Data Set S4). Compiled endmember source values are taken from Damodararao et al. (2016). Major rivers are marked in blue: Gang., Ganges; Brah., Brahamaputra; Maha., Mahanadi; Goda., Godavari; Kris., Krishna; Irra., Irrawaddy; Salw., Salween; NBS., Namche Barwa Syntax; S, Siang; D, Dibang; L, Lohit. Major geological units and their Nd isotope composition (after Galy & France-Lanord, 2001): Sub. H., Sub Himalaya; LH, Lesser Himalaya εNd −25; HHC, High Himalayan Crystalline εNd −16; TSS, Tethys Himalayan sedimentary εNd −12 to −4, the Transhimalayan plutonic belt rocks are found around the IYSZ, Indus-Yarlung Suture Zone; LB, Lhasa Block; QB, Qiangtang Block; SGB, Songpang Ganza Block. (b) Modern JJAS mean precipitation (mm/day) for the period 1979–2015 (GPCC precipitation data provided by the NOAA/OAR/ESRL PSD and can be accessed at https://www.esrl.noaa.gov/psd/).

climate is limited by a lack of continuous records from the South Asian Monsoon (SAM) region with well-constrained age control extending back into the Oligocene (e.g., Clift & Webb, 2019).

The unique land-sea configuration of the Indian Ocean and the HTP is key to the evolution of the Asian monsoon system in that it controls the spatial pattern of atmospheric circulation and the regional hydrology of Asia (Clemens & Oglesby, 1992; Zhao & Moore, 2004). The vast majority of south and east Asian monsoon rain occurs during the SW summer monsoon from June to September (Figure 1). These feed the Asian rivers which deliver huge amounts of sediments (>50% of global fluxes) into the northern Indian Ocean and the South China Sea (Milliman & Syvitski, 1992). The Bay of Bengal (BoB) has received discharge and sediments from the Ganga and Brahmaputra rivers (G-B) draining the Himalayas since the Eocene (Najman et al., 2008) resulting in the largest accumulation of sediment on the planet, the Bengal Fan (Curray et al., 2003). The BoB also receives sediments from Indian peninsular rivers and the Irrawaddy and Salween rivers (I-S), which, although most of their load is deposited in the Andaman Sea, are significant sediment suppliers (I-S load ~70% of G-B) (Chapman et al., 2015) draining geological formations similar to the Brahmaputra. The small rivers of the Arakan coast draining the Indo-Burman Ranges are poorly studied but the Sr and Nd isotope compositions of surface sediments reveal that they are an important source of material to the eastern BoB (Figures 1 and 2; Colin et al., 1999).

Radiogenic Sr ($^{87}Sr/^{86}Sr$), Nd ($^{143}Nd/^{144}Nd$, expressed as εNd) and Pb ($^{206}Pb/^{204}Pb$, $^{207}Pb/^{204}Pb$, $^{208}Pb/^{204}Pb$) isotope compositions reflect rock type and age and are widely used as provenance tracers (Frank, 2002; Hemming & McLennan, 2001). The geological formations of the continental areas surrounding the Bay of Bengal are characterized by large differences in radiogenic isotope compositions, which allow the detailed distinction of sediment sources (e.g., Galy & France-Lanord, 2001, Figures 1 and 2). Analyses of modern river sediments reveal that a disproportionally large fraction (compared to drainage area) of the sediments in the lower Meghna river, after the confluence of the Ganga and Brahmaputra, originate from the latter (Galy & France-Lanord, 2001). This has been attributed to higher monsoon rainfall over parts of the Brahmaputra catchment driving enhanced erosion (Figure 1). Intense erosion and incision around the Namche Barwa syntax of the Siang tributary and the eastern tributaries (Dibang & Lohit), where average annual rainfall is > 3 m/yr, results in a high contribution from the rocks of the Transhimalayan plutonic belt to the downstream Brahmaputra sediments (Singh & France-Lanord, 2002). The isotope composition of BoB surface sediments exhibit a pronounced east-west divide (Colin et al., 1999; Figure 1a) with more radiogenic Nd isotope signatures in the eastern part reflecting input from the Indo-Burman Ranges, where monsoon rainfall is also particularly intense (Figure 1b; Damodararao et al., 2016).

The monsoon-related erosional history of the Himalayas has been reconstructed in the geological past based on the Sr and Nd isotope compositions of Bengal Fan sediments that accumulated over the last 12 (Galy et al., 2010) and 16.5 Myrs (Derry & France-Lanord, 1996). However, these records do not include the postulated initiation or strengthening of the monsoon in the early Miocene (Clift et al., 2008; Guo, 2002) and the discontinuous deposition of the Fan sediments by turbidity currents and

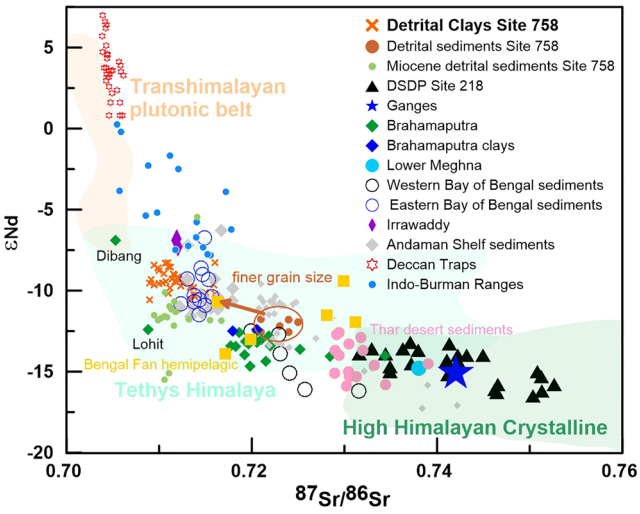

Figure 2. Nd-Sr isotope compositions of the clay size fraction of Site 758 compared with literature data (sources and details in Data Set S4) for bulk silicate sediments from the same site, surface marine sediments of the Bay of Bengal and possible source areas. Bengal fan data (Galy et al., 2010; Hein et al., 2017): Generally plot in the HHC field but hemipelagic sediments (yellow squares) from the fan plot with the Ninety East Ridge bulk detrital silicates and clay size fraction confirming that these values are representative for the entire basin. Bulk detrital silicate isotope compositions of ODP Site 758 sediments are also shown and the offset between these values and the clay size data allows estimation of the grain size effect (see Figure S1). The fields for three major Himalayan rock formations are after Gourlan et al. (2010).

the high abundance of sand limit the constraints for age control. Here, we instead utilize the continuous sedimentary sequence of ODP Site 758 (Figure 1) on the Ninety East Ridge, which has a well-constrained stratigraphy that has recently been updated and improved based on results from a new drill Site (IODP Site U1443) at the same location (Clemens et al., 2016) (see Section 2). We reconstruct the sources of clay minerals, which are the product of silicate weathering in the core SAM region of the past 27 Myrs and find that the regions with the highest monsoon rainfall today have been weathered persistently over this time.

2. Materials and Methods

Ocean Drilling Program (ODP) Site 758 is located on the southeastern side of one of the large en echelon blocks that characterize the Ninety East Ridge between the equator and 10°N. The core was retrieved from a water depth of 2,924 m, about 1,000 m above the Bengal Fan in the southern Bay of Bengal (5° 23.05′ N, 90° 21.67′ E; Figure 1b). Site 758 was cored to 677 m below seafloor and recovered Upper Cretaceous to recent sediments (Pierce et al., 1989). Here, we only focus on the upper 234 m to reconstruct the SAM history from the Oligocene to the present. In December 2014 International Ocean Discovery Program (IODP) Expedition 353 drilled Site U1443 close to ODP Site 758. The continuous recovery enabled by multiple holes into the Oligocene at Site U1443 allowed significant improvement of the ODP Site 758 age model, especially during the early and middle Miocene. To import the new Site U1443 calcareous nannofossil and paleomagnetic age constraints, ODP Site 758A cores were correlated to Site U1443 A at the meter scale using color line scan data from U1443 A and RGB data extracted from composite core images of ODP Site 758 (Figure S3) with macros written by Roy Wilkens (https://www.codd-home.net/) for Igor ProTM (https://www.wavemetrics.com/index.html). During the middle Miocene (8.5–14 Ma), we use the age tie points from the high-resolution benthic foraminifer carbon and oxygen isotope stratigraphy from Site U1443 (Lübbers et al., 2019). Linear sedimentation rates fitted through all the age points were employed from the Pleistocene to Mid-Miocene and again in the early Miocene to Oligocene (Figure S4). Further details of the new age model are provided in the supplement.

In total, 38 samples (Table S3), were selected for the analysis of radiogenic Sr, Nd, and Pb isotopes of the clay-size fraction and for the determination of clay mineral assemblages following Ali et al. (2015). Sediment samples were first freeze dried and then wet sieved over 63 μm and the <63 μm size fraction were further processed to separate clays (<2 μm). Carbonates and organic matter were removed by leaching for 12 h (with 30 min in an ultrasonic bath) with 1.5 M acetic acid and 10% H_2O_2. This was repeated several times until all carbonates were removed and no further reaction was observed. In a second step 0.05 M hydroxylamine hydrochloride and 2.6 M acetic acid solution buffered to pH 3.6 with NaOH was used to remove Fe-Mn oxyhydroxide coatings by leaching for 1 h in an ultrasonic bath and for 2 h on a shaker. This was followed by a triple rinse with de-ionized water to remove the soluble fraction. A centrifuge based Atterberg method was used to separate the clay-size fraction (<2 μm) which was confirmed by analyzing a subset of samples with a laser diffraction particle size analyzer (Beckman Coulter) LS I3 320. Finally, the separated clay samples were freeze-dried before total dissolution or X-Ray Diffractometer (XRD) analysis.

About 100 mg of the dried clays were completely dissolved using mixtures of concentrated HF-HNO3-HClO4. The separation and purification of Sr, Nd, and Pb followed previously established procedures in our lab (e.g., Ali et al., 2015). Sr, Nd, and Pb isotope compositions were measured on a Nu Plasma MC-ICP-MS at GEOMAR. Mass bias for $^{87}Sr/^{86}Sr$ was corrected with an $^{88}Sr/^{86}Sr$ of 0.1194 and values normalized to the accepted value of NIST NBS987 of 0.710245. The 2σ reproducibility for $^{87}Sr/^{86}Sr$ of NBS987 was ±0.00004 and repeated processing and analysis of USGS marine sediment reference material MAG-1 (n = 20) gave a mean $^{87}Sr/^{86}Sr$ value of 0.722873 ± 0.00003 (2σ) which agrees well with the values reported

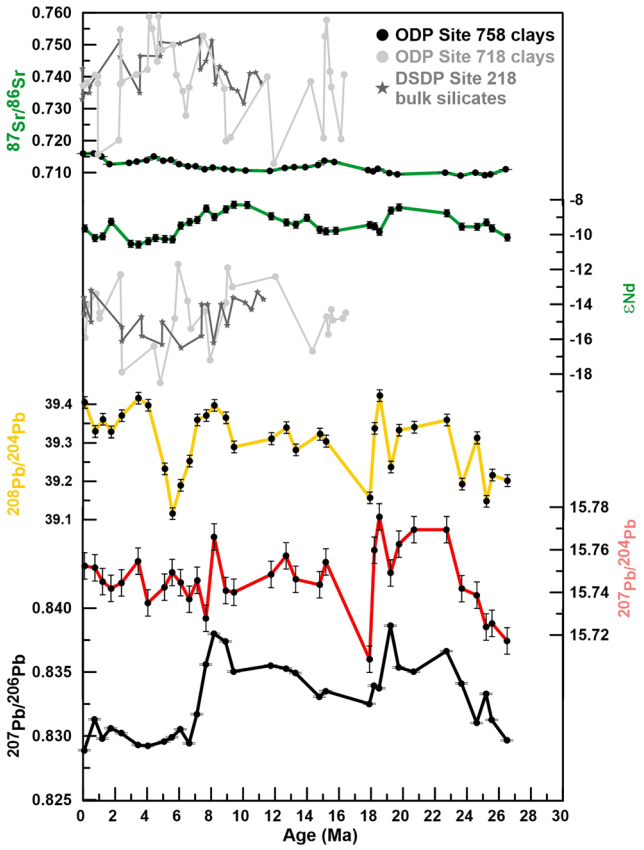

Figure 3. Clay fraction Sr, Nd and Pb isotope records of ODP Site 758 on the Ninety East Ridge with comparable records from the adjacent (DSDP Site 218) (Galy et al., 2010) and distal Bengal Fan (ODP Site 718) (Derry & France-Lanord, 1996). Error bars represent the external 2σ reproducibility of the data based on the repeated measurement of the MAG-1 marine sediment reference material.

by Nath et al. (2009) (0.722739). $^{143}Nd/^{144}Nd$ ratios were mass-bias corrected with $^{146}Nd/^{144}Nd = 0.7219$ and normalized to the accepted value of the JNdi-1 standard of 0.512115 (Tanaka et al., 2000). Repeated measurements of an in-house Nd standard "SPEX" gave a reproducibility of ±0.20 εNd units (2σ). Repeated processing and analyses of reference material MAG-1 ($n = 21$) gave a mean εNd value of −11.2 ± 0.2, agreeing with the values reported by Nath et al. (2009). Blanks were typically below 60 pg for Nd and 1.8 ng for Sr and hence well below 1% of the sample mass. A standard-sample bracketing method was used to determine the Pb isotope ratios. The 2σ reproducibility for the Pb NIST NBS981 standard was ±0.0152, ±0.0062, ±0.0064, and ±0.00006 for $^{208}Pb/^{204}Pb$, $^{207}Pb/^{204}Pb$, $^{206}Pb/^{204}Pb$ and $^{207}Pb/^{206}Pb$, respectively. Blanks were typically below 250 pg so that blank contributions to the Pb analyses can be neglected. Repeated processing and analysis of MAG-1 ($n = 16$) gave a mean value ±2 standard deviations of 38.811 ± 0.011, 15.658 ± 0.003, and 18.863 ± 0.002 for $^{208}Pb/^{204}Pb$, $^{207}Pb/^{204}Pb$, and $^{206}Pb/^{204}Pb$, respectively. These Pb isotope values agree well with those previously reported for MAG-1 (Nath et al., 2009).

For the determination of clay mineral assemblages the separated clay-size fraction (<2 μm) was suspended in an ultrasonic bath and placed on 0.2 μm filters by applying a vacuum below the filters. The XRD runs were performed following glycol-dehydration for 24 h. The analyses were conducted using a Phillips X-Ray diffractometer (PW series) with CoKα radiation and a Ni filter under a voltage of 40 kV and an intensity of 35 mA. The relative amount of each clay mineral was estimated according to the position of the (001) series of the basal reflections on the XRD diagrams that is, smectite (001) at 17 Å, illite (001) at 10 Å, kaolinite (001), and chlorite (002) at 7 Å. Kaolinite and chlorite were discriminated according to the relative proportions deduced from the ratios of the 3.57 Å and 3.54 Å peak areas. One sample was measured several times ($n = 5$) and the reproducibility of the semi-quantitative clay mineral analysis was ±2% (1σ). Although the leaching steps to isolate silicates are not always performed prior to clay mineral analysis similar clay mineral results have been obtained in the region without leaching (see supplementary discussion) and only the relative changes in clay minerals should be interpreted.

3. Results

The Sr, Nd, and Pb isotope compositions measured on the clay-size fraction are provided in Data Set S1 and are displayed in Figures 2–4. The $^{87}Sr/^{86}Sr$ ratios range from 0.709 to 716 (average 0.712) whereas the εNd values vary from −10.6 to −8.3 (average −9.5). The Pb isotope compositions show a range of variations: $^{208}Pb/^{204}Pb$ from 39.116 to 39.422, $^{207}Pb/^{204}Pb$ from 15.709 to 15.775, and $^{206}Pb/^{204}Pb$ from 18.779 to 19.003. Compared to the different source lithologies these ranges are remarkably narrow. Although exhibiting different absolute values and a smaller range, the data from the Ninety East Ridge clays record similar trends to those observed in clays and bulk sediments from the Bengal fan (Figure 3). The results of the clay mineral analyses are listed in Data Set S1 and displayed in Figure 5. Illite, chlorite, smectite and kaolinite are present in all analyzed samples. Illite and chlorite contents vary from 3% to 27% (average ~12%) and 0%–19% (average ~6%), respectively. Smectite is the dominant clay mineral ranging from 39% to 69% (average ~56%). The abundance of kaolinite varies from 11% to 46% (average 26%).

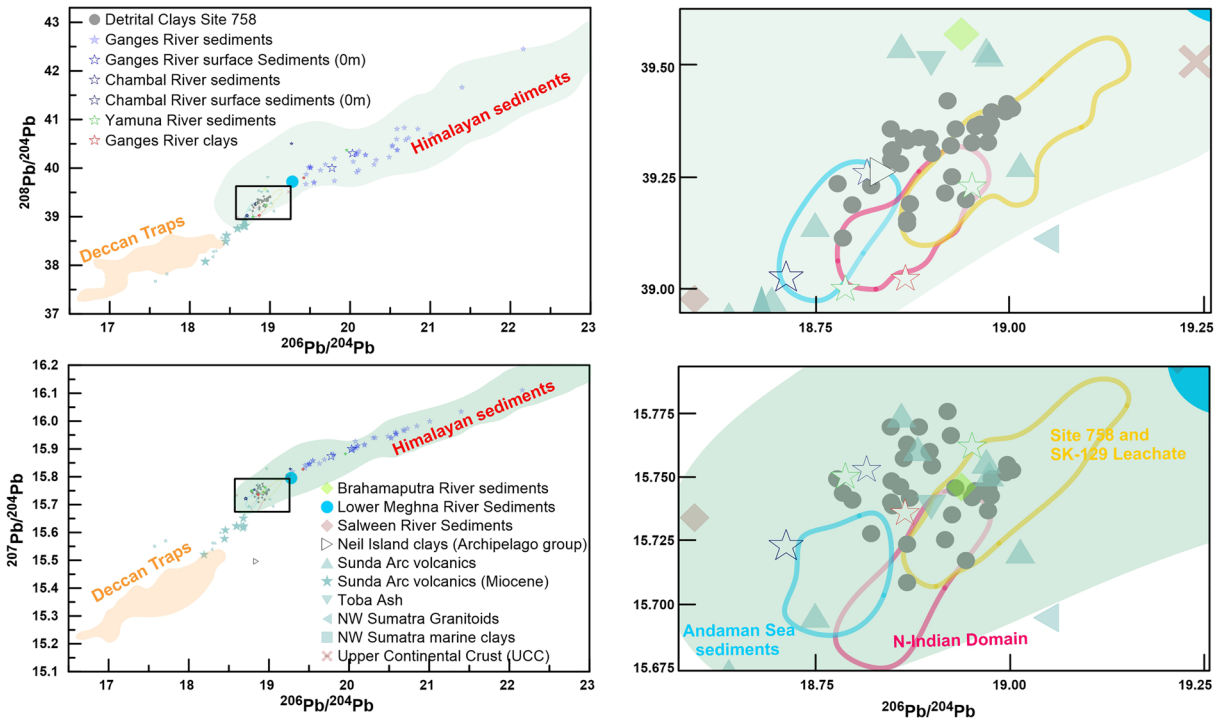

Figure 4. $^{208}Pb/^{204}Pb$-$^{206}Pb/^{204}Pb$ and $^{207}Pb/^{204}Pb$-$^{206}Pb/^{204}Pb$ diagrams for ODP Site 758 clays and potential sources (details in Data Set S4) including Ganga, Brahmaputra and Lower Meghna sediments. Red triangles represent northern Deccan Traps basalts while green triangles show the compositions of Himalayan sediments and the Indian shield.

4. Discussion

4.1. Provenance of Bay of Bengal Clays

Analyzing the radiogenic isotope composition of the clay size (<2 microns) fraction minimizes transport-related grain size effects (Figure 2; Derry & France-Lanord, 1996) that influence the composition of the detrital sediments at the Ninety East Ridge (Ahmad et al., 2005). Considering the wide range of ages and types of rocks surrounding the BoB (Figure 1), the variations in isotope composition of the clays are small (Figure 2) suggesting that the mixture of sources of detrital clays to the Ninety East Ridge has remained remarkably constant over the past 27 Myrs (Figure 2). The Himalayas themselves are composed of mostly the same sequence of rocks (TSS and HHC) so would provide mixtures of sediment with similar isotopic compositions. This is consistent with active Himalayan erosion for the last 38 Myrs (Najman et al., 2008) and confirms and extends results from the Bengal Fan suggesting a constant Himalayan source of material for the last ~16 Myrs (Derry & France-Lanord, 1996; Galy et al., 2010).

However, the Ninety East Ridge clays are clearly not exclusively Himalayan in origin as they are characterized by more radiogenic Nd and less radiogenic Sr and Pb isotope signatures than Himalayan rocks and most Bengal Fan sediments (Figures 2 and 4). Direct comparison of our clay fraction isotope signatures to river sediment data from the literature is potentially complicated by grain size dependent mineral sorting given that very few of these analyses were performed on clay size separates. The few measurements of the clay size fraction of Brahmaputra sediments indicates clays have slightly more radiogenic Nd compositions compared to bulk river bed sediments (Singh & France-Lanord, 2002) between 0.2 and 0.9 eNd units more radiogenic and with $^{87}Sr/^{86}Sr$ values 0.002 to 0.02 more unradiogenic. Similar differences between clay size and bulk sediment Sr and Nd isotopes have been found in the turbidite sediments of Himalayan origin delivered by the Indus to the Arabian Sea (Carter et al., 2020). Comparison of clay isotope compositions with bulk detrital measurements from similarly aged sediments at the same core location suggests the grain size influence ranges between 2.3 and 2.4 epsilon units for Nd and between 0.0001 and 0.008 for $^{87}Sr/^{86}Sr$ ratios (Figure S1). Considering these differences the main sources of clays at the Ninety East Ridge over the

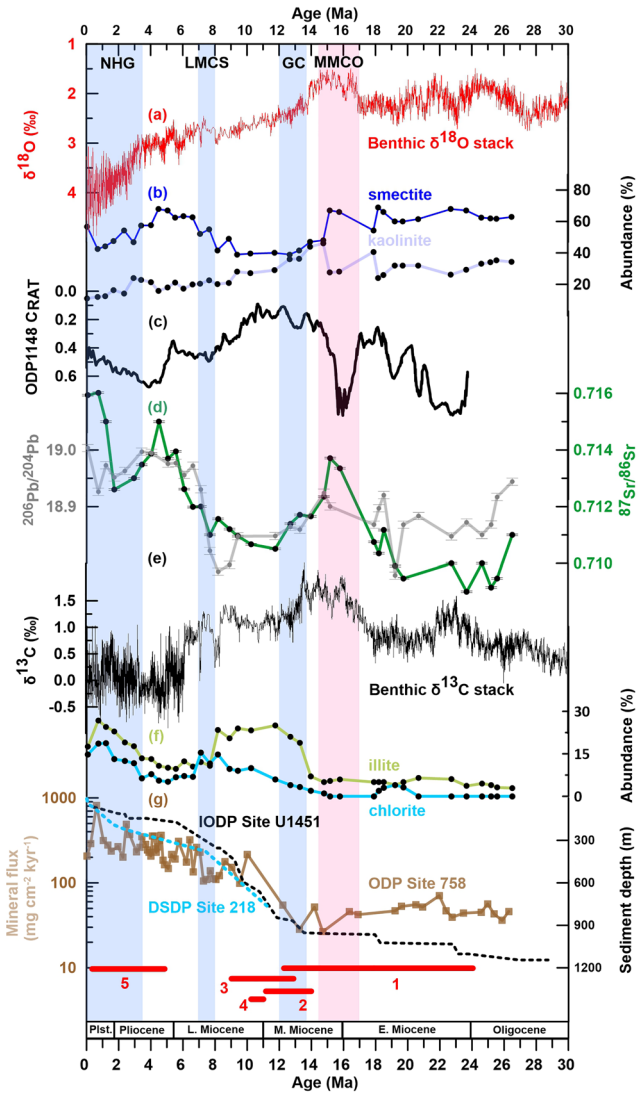

Figure 5. (a and e) Global $\delta^{18}O$ and $\delta^{13}C$ from bottom living (benthic) foraminifera compiled from more than 40 DSDP and ODP sites (Zachos et al., 2008) represents global ice volume and deep sea temperature highlighting the global climate changes of the last 30 Myrs. Periods of global cooling, after Zachos et al. (2008) are marked with blue bars, and the Middle Miocene Climate Optimum is marked with a red bar (b and f). Clay mineralogy of ODP Site 758, relative abundances (%) of Smectite, and Kaolinite, Illite, and Chlorite), (c) CRAT record of ODP Site 1148 (Clift et al., 2008) from the South China Sea as a record of East Asian Monsoon development, (e) Nd and Pb isotope composition of ODP Site 758 clays (g) mineral flux record (Hovan & Rea, 1992) of ODP Site 758 recalculated using updated linear sedimentation rates from the new age model (see supporting information), and sedimentation rates from the Bengal fan DSDP Site 218 and IODP Site U1451 (France-Lanord et al., 2016; Galy et al., 2010) and at the bottom a summary of the regional tectonic events (Allen & Armstrong, 2012). 1, High Himalayan Uplift, Main Central Thrust (MCT); 2, Onset of normal Fault, South Tibet; 3, Surface Uplift East Tibet; 4, Initial thrusting on Main Boundary Trust; 5, Fast exhumation at Himalayan syntaxes, Outward growth of NE Tibet. The ages of literature data plotted have been updated to the more recent GTS12 time scale (Gradstein et al., 2012).

past 27 Myrs have been the Brahmaputra and the Irrawaddy/Indo-Burma Ranges (IBR) (Figure 2). Bengal Fan silicates generally plot in the High Himalayan Crystalline (HHC) field but samples from hemi-pelagic fan sediments plot close to the Ninety East Ridge bulk detrital silicates and the clay size fraction (Galy et al., 2010) clearly indicating that the radiogenic isotope signatures of the Ninety East Ridge clays reflect the fine-grained sediment supplied to the basin (Figure 2).

The eastern Brahmaputra tributaries and the IBR (via Arakan coast and Irrawaddy rivers) are the most likely sources of the radiogenic Nd isotope signature of the Ninety East Ridge clays given that contributions from other highly radiogenic sources such as the Deccan Traps or Sumatra are unlikely as discussed below. Compared to Sr and Nd there are few Pb isotope data in the literature for the region but Pb isotopes are more sensitive to crustal processes (Hemming & McLennan, 2001) and some data for the suspended sediments from the Ganges, Brahmaputra, and Lower Meghna rivers are available (Figure 4). The Pb isotope compositions of the clays plot at the lower end of the Himalayan river sediments and show a close similarity to those of the Brahmaputra supporting our Sr and Nd isotope results (Figure 4).

Although a wide range of Sr, Nd and Pb isotope values have been reported for the Deccan basalts (Data Set S4) this is mostly the result of lithospheric contributions in the magmas of the early lava flows (e.g., Lightfoot et al., 1990). The younger and more voluminous flows all have highly radiogenic εNd (unradiogenic$^{87}Sr/^{86}Sr$) and distinctly unradiogenic Pb isotope signatures (Figure 4), precluding a significant Deccan contribution to the Ninety East Ridge clays, as suggested previously for distal fan clays (France-Lanord et al., 1993). The distribution of Deccan basalt-derived clays from Indian peninsular rivers is likely to restricted to the Indian margin by the monsoon-induced Indian coastal current (Kumar et al., 2006). In addition, the sediment load of the peninsular Indian rivers draining the Deccan basalt areas (246 Mt/year compiled load of Krishna, Godavari and Mahanadi) (Milliman & Syvitski, 1992) are simply swamped by the big rivers (G-B and I combined supply 1320 Mt/year) (Milliman & Syvitski, 1992; Robinson et al., 2009). Such a vast amount of suspended sediment also means that the potential influence of fine-grained mineral dust in this region is small with identified continental dust sources either being the Ganges plain with Himalayan provenance (Tripathi et al., 2013) (Thar dessert Figure 2) or air masses from SE Asia with low mineral dust loadings (e.g., Srinivas & Sarin, 2013).

Another proximal and therefore potential source is the Sunda arc (Figure 1), but material from this source is unlikely to reach the Ninety East Ridge given the prevailing SW or NE winds and ocean currents in the Andaman Sea. A wide range of isotopic values have been reported for Sumatran volcanic rocks as some of the most recent lavas bear a signature of crustal contamination and inclusion of subducted sediments (e.g., Gertisser et al., 2003). However, compared to the age of our sediment record these volcanic rocks are young (Quaternary) and Miocene and older Sumatran formations (and also some Quaternary/Pliocene volcanics) exhibit more radiogenic εNd (unradiogenic $^{87}Sr/^{86}Sr$) and distinctive Pb isotopes (Figure 4), making a significant supply of material from Sumatra unlikely. Furthermore, over the course of the last 30 Myrs, the NER has moved closer and closer to Sumatra (Hall, 2012) and the shallow shelves

surrounding Sumatra have been repeatedly exposed and flooded (Zahirovic et al., 2016), either presenting easily erodible material or trapping sediment. Such changes should have strongly affected any possible sediment supply from Sumatra are not consistent with the remarkably invariable radiogenic isotope composition of Ninety East Ridge clays over the last 27 Myrs. Instead, like the sedimentary rocks of the Andaman Islands and the Nicobar fan (Awasthi & Ray, 2020; Chen et al., 2020; McNeill et al., 2017), the source of detrital sediments to the Ninety East Ridge has been dominated by sources from the north where SAM rainfall and exhumation are most intense.

4.2. Clay Mineralogy

Secondary clays formed during silicate weathering dominate the clay mineral assemblage (Data Set S1) with smectite ranging from 39% to 69% (average ~56%) while the abundance of kaolinite varies from 11% to 46% (average 26%). Illite (average ~12%) and chlorite (average ~6%) are primary minerals derived by physical erosion of the Himalayan formations (France-Lanord et al., 1993). Analyses of Brahmaputra suspended sediments have revealed that the <2 μm fraction only represents 0.5%–3% and is composed of illite, vermiculite and chlorite, but no detectable kaolinite or smectite (Singh & France-Lanord, 2002). Near the confluence with the Ganga, and in delta sediments, secondary clays are found (Heroy et al., 2003). This strongly suggests that the secondary clay minerals formed by silicate weathering occurring in the floodplain (France-Lanord et al., 1993) where smectite can preferentially form in poorly drained soils (Alizai et al., 2012; Thiry, 2000). The primary clay minerals have been eroded, transported and possibly stored in the floodplain, while the secondary clays formed in floodplain soils, before being eroded and transported to the Ninety East Ridge. The timescales of these processes are poorly constrained (Thiry, 2000), but changes in Holocene clay mineralogy on the floodplain seem to be climatically controlled (Heroy et al., 2003) and recent work on the Ganga river suggests minimal floodplain storage (Lupker et al., 2011). In view of the million-year resolution record presented here, any potential time lag should be negligible.

A smectite content >39% could indicate a strong contribution from volcanic rocks like the Deccan trap basalts but clays from the Indus floodplain also have relatively high-smectite contents without substantial amounts of volcanic rocks in the basin (Alizai et al., 2012). The isotopic data and the considerations above argue against a major Deccan trap contribution as established for the smectite rich clay layers from the distal Bengal Fan based on major and trace elements (Fagel et al., 1994) and stable isotope compositions (France-Lanord et al., 1993). Some instances of authigenic smectite have been reported in biogenic opal rich sediments from the central Indian Ocean with acid leaches of clay sized sediments having an isotope composition similar to Indian Ocean seawater (Fagel et al., 1997). A significant seawater contribution to the Ninety East Ridge clays can be ruled out given that the $^{87}Sr/^{86}Sr$ measured on the strongly pre-leached clays (carefully removing authigenic phases except for possibly some barite) of this study is always higher than that of contemporary and Miocene seawater (McArthur et al., 2001) and neither the clay $^{87}Sr/^{86}Sr$, nor the offset between clay and contemporaneous seawater $^{87}Sr/^{86}Sr$, correlates with the smectite content (Figure S2). Although some reverse weathering likely occurs on the shelf (Michalopoulos & AIIer, 1995), the Sr incorporated (and by inference the Nd and Pb as well given that seawater Sr concentrations are much higher) into these clays is sourced from the river sediments and not seawater. Furthermore, the smectite content is also high in Pleistocene turbidite sediments from sea level low stands in the northern BoB (Joussain et al., 2016) suggesting the smectite rich clays were eroded from the shelf sediments from the eastern BoB. Although smectite can be preferentially scavenged during flocculation in the estuary as inferred for the Indus (Li et al., 2019) if it escapes to or is formed on the shelf it can preferentially remain in suspension compared to other clay minerals (Chamley, 1989). Transport processes clearly influence the clay mineralogy of Bengal Fan surface sediments (Li et al., 2017) but such fine material will remain in suspension until flocculated or incorporated into larger particles (Milligan & Hill, 1998). The deposition of fine clays on the Ninety East Ridge is linked to productivity and the sinking of biogenic particles as the seasonal variability of the lithogenic flux to sediment traps in the southern BoB follows the carbonate and opal fluxes peaking during the summer monsoon months (Unger et al., 2003). Such a deposition process is unlikely to selectively influence the clay size mineralogy. Although the Himalayas and river mouths were further away in the early Miocene (Hall, 2012; Najman et al., 2008) the detrital mineral flux to the site was elevated compared to more distal sites in the Indian Ocean with similar sedimentation rates (Hovan & Rea, 1992) demonstrating the persistence of enhanced continental weathering inputs to the BoB. A final consideration is the occurrence

of ash layers that could weather to smectite in the sediments. We were careful not to sample any ash layers and the occurrence of ash layers does not start until the middle Miocene and increases into the Pleistocene (Pierce et al., 1989), opposite to the pattern of decreasing smectite abundance observed in the middle Miocene core section. Therefore, we are confident that our clay mineral assemblages represent weathering processes in the big river basins, albeit passed through the filter of transport to the Ninety East Ridge.

4.3. SAM Induced Silicate Weathering

The radiogenic isotope signatures suggest that silicate weathering in the Brahmaputra and IBR regions supplied the vast majority of the clays to the Ninety East Ridge over the past 27 Myrs (Figure 2). Today these are the locations of the highest monsoon rainfall over South Asia (Figure 1b). We do not interpret any subtle changes in the mixture of sources given that these would be ambiguous in view of the range in source rock compositions (Figures 2–4). However, there is a clear shift in both Sr and Pb isotope compositions around 8 Ma which is not clearly mirrored by the Nd isotope signatures suggesting incongruent weathering effects as opposed to source changes (Frank et al., 2002). For example the preferential weathering of biotite under cooler climates would result in clay minerals with higher $^{87}Sr/^{86}Sr$ (Li et al., 2007) and radiogenic Pb isotopes are also preferentially released from the first minerals weathering chemically (Harlavan et al., 2009). However, these changes in Sr and Pb isotopes are subtle (Figures 2–4) and the apparently stable spatial distribution of silicate weathering during the major tectonic reorganizations of the Miocene (e.g., Allen & Armstrong, 2012) argues for SAM precipitation as the primary control on regional erosion and weathering, although precipitation is closely related to relief in the region today (Damodararao et al., 2016). We can constrain the rock types and ages being weathered but the location of the weathering may have changed over time. The processes of erosion and silicate weathering can be separated in both time and space, for example, the IBR consist of sediments produced by the erosion of the Himalayas (Licht et al., 2013) that are weathered under a wet tropical climate. Sedimentary rocks with IBR composition have contributed a large portion of the clays produced by silicate weathering and transported to the Ninety East Ridge over the last 27 Myrs but the location of the weathering may have changed as the formations were eroded, deposited and uplifted to form the IBR (Najman et al., 2020). Although the Lesser Himalayan (LH) lithologies have been exposed to erosion since approximately 16 Myrs ago (Colleps et al., 2018) the isotopic constraints indicate the LH contribution to the Ninety East Ridge clays must be very small. The products of Himalayan erosion deposited on land (Siwaliks) and on the Bengal fan also do not exhibit a significant contribution from these formations with highly unradiogenic Nd isotope signatures (Galy et al., 2010; Galy & France-Lanord, 2001). In the western Himalaya the delivery of LH material to the Indus fan occurred only in the Pliocene, later than in the foreland basin records (Clift et al., 2019). Although the LH rocks currently contribute a large proportion of the dissolved Sr content of the Ganga river during the monsoon months (Bickle et al., 2005), the minimal LH signals in the regional weathering products of the last few million years suggests that the radiogenic Sr isotope composition of seawater was a more reliable recorder of continental silicate weathering than often considered (e.g., Colleps et al., 2018). Ultimately the provenance of clay minerals documented here may differ from silicates eroded and transported by turbidity currents to form the Bengal and Nicobar fans (e.g., Chen et al., 2020; Najman et al., 2019). While the fan deposits record the sources of eroded material, the clays are dominated by secondary minerals formed in the weathering environment and changes in the formations being eroded may not be synchronous with changes in chemical silicate weathering.

Having confirmed the stable source provenance of clay minerals at the Ninety East Ridge with their radiogenic isotope signals, the clay mineralogy provides additional information on the weathering regime and climate of the source region (France-Lanord et al., 1993). Kaolinite forms under hot and humid tropical weathering with strong hydrolysis (e.g., Chamley, 1989) and the kaolinite percentage in Ninety East Ridge clays has decreased only modestly as global climate cooled (Figure 5b). This indicates that tropical weathering persisted in the watersheds with the strongest monsoon rainfall today and was even more prevalent in the late Oligocene and early Miocene. Smectite abundance was variable but has remained high throughout the last 27 Myrs. Data from an experimental catchment in the monsoon dominated Western Ghats found smectite dissolution/precipitation to be the main control of the chemical weathering flux of dissolved Si (Violette et al., 2010). Smectite is not stable in a climate with high precipitation (>900 mm/yr) but instead forms under semi-arid conditions (900–500 mm/yr). Under the current climate in the Western

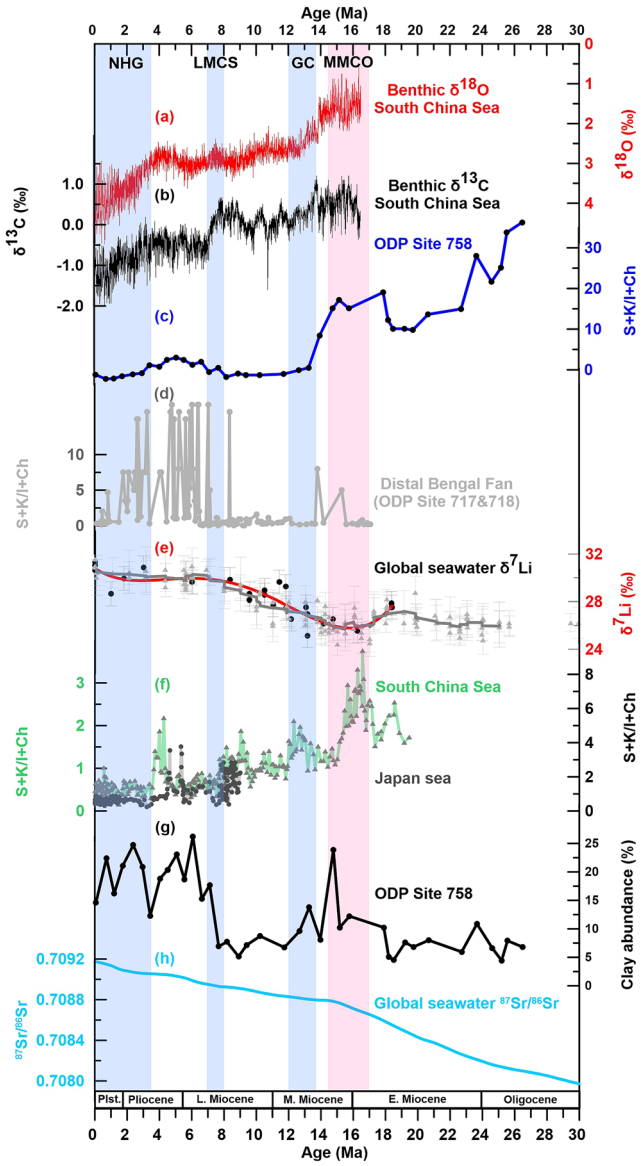

Figure 6. (a and b) $\delta^{18}O$ and $\delta^{13}C$ from benthic foraminifera records from composite sequence of Holes 1146A and 1146C from South China Sea (Holbourn et al., 2018) represents ice volume and deep sea temperature highlighting the global climate changes of the last 16 Myrs. The age model for Site U1443 and therefore the samples from Hole ODP Site 758 used here have been directly tied to these high resolution records of middle Miocene climate change (Lübbers et al., 2019). Periods of global cooling, after (Zachos et al., 2008) are marked with blue bars, and the Middle Miocene Climatic Optimum is marked with a red bar. (c and d) Clay mineralogy of ODP Site 758 S + K/I + Ch (Smectite + Kaolinite)/(Illite + Chlorite) compared with ODP Sites 717 & 718 (Bouquillon et al., 1990) (e) Seawater Li isotope records from planktic foraminifera replicated in different ocean basins as a tracer of global silicate weathering intensity (Hathorne & James, 2006; Misra & Froelich, 2012) (f) Clay mineral records of ODP Site 1146 in the South China Sea (Wan et al., 2007) and IODP Site U1430 from the Japan Sea (Shen et al., 2017) (g) Global seawater Sr isotope record compiled by McArthur et al. (2001).

Ghats smectite dissolves and kaolinite precipitates. Therefore, the higher kaolinite abundances during the late Oligocene and Miocene strongly suggests that more regions received rainfall >900 mm/yr.

4.4. Middle Miocene Increase in Physical Weathering

The most prominent change in the clay minerals delivered to the Ninety East Ridge was the pronounced increase in the primary minerals illite and chlorite around 13.9 Ma (Figure 5f) accompanying a major global cooling step (Figure 5a). This was also coincident with the start of the major increase in detrital mineral flux to the site (Figure 5g) but the change in illite content experienced a much sharper transition while chlorite abundance increased gradually (Figure 5f). The marked increase in detrital mineral flux to ODP Site 758 was originally interpreted to represent the start of monsoon induced erosion and weathering but may also have resulted from the progradation of the Bengal Fan reaching a point where suspensions originating from turbidity flows were able to reach the top of the Ninety East Ridge. There were coeval increases in sedimentation at the nearby drill sites on the Bengal Fan (Figure 5g) while the Nicobar fan on the other side of the Ninety East Ridge only started accumulating rapidly after 9.5 Ma (McNeill et al., 2017). Industry wells on the western Bengal Fan suggest that sedimentation rates were high throughout the Miocene (Krishna et al., 2016) suggesting a major shift in the location of sediment deposition during the Miocene is unlikely. If these few long drill holes are representative, this suggests that the mid Miocene increase in the supply of detrital minerals to the Ninety East Ridge represents a general increase in supply to the BoB region.

The secondary (Smectite + Kaolinite) over primary (Illite + Chlorite) clay mineral ratio is a measure of chemical versus physical weathering (Figure 6) and is of particular interest in the BoB given that the amount of organic carbon buried in the Bengal Fan is more than 3 times greater in smectite-kaolinite dominated sediments compared to illite-chlorite sediments (France-Lanord & Derry, 1997). After the increase in primary clay mineral supply in the middle Miocene, the changes in primary clay mineral abundance on the Ninety East Ridge exhibit a similarity to the East Asian Monsoon record from the South China Sea (Clift et al., 2008) suggesting that the peaks in physical erosion were related to a generally strong monsoon across Asia (Figure 5). Although the result of different transport pathways, a similar shift to a more primary clay mineral dominated assemblage (also without major source changes) was also observed during the Miocene in the South China Sea (Wan et al., 2007) and Sea of Japan (Shen et al., 2017; Figure 6), suggesting that this is a regional signal and likely of global importance. Although we observe a strong increase in physical erosion with global cooling across the Asian monsoon region, secondary clay minerals formed by silicate weathering still dominate and silicate weathering persisted in the same regions with the highest monsoon rainfall as today over the last 27 Myrs. This persistence may point to a tectonically driven control where rainfall follows orography and exhumation drives more uplift (e.g., Thiede et al., 2004) but the system is buffered by the vast amounts of sediments available for weathering supplied by the Himalayan orogeny.

4.5. SAM Intensity, Silicate Weathering Regime and Global Climate

The clay mineral data indicate that weathering was more intense under warmer and wetter Miocene climates and decreased slightly as global climate cooled, but what are the implications for the monsoon intensity in the past? This question is difficult to answer as monsoon intensity can be defined based on the amount of precipitation, the seasonality of precipitation, or wind speed and direction. The monsoon today is a seasonal phenomenon with the monsoon climate being characterized by a relatively dry climate for two thirds of the year. Many lines of evidence interpreted as the start of the SAM occurred around either the mid-Miocene global cooling (e.g., Betzler et al., 2016) or the late Miocene global cooling (e.g., Quade et al., 1989), but other records point to a decrease in weathering or precipitation during the late Miocene in the SAM and EAM regions (Clift et al., 2008; Holbourn et al., 2018; Steinke et al., 2010). One way to reconcile these seemingly disparate views is that these changes represent the development of the dry season between monsoon rains and the NE winter monsoon, like inferred for the late Miocene in east Asia (Holbourn et al., 2018). In the SAM domain it appears that the emergence of the dry season accompanied middle Miocene global cooling while the late Miocene saw increases in secondary clays and clay abundance on the Ninety East Ridge and secondary clays in the distal Bengal fan (Figures 5 and 6), implying increased silicate weathering. However, the records of vegetation change recorded in the Siwalik deposits across the Himalayas suggest the aridification was more pronounced in the west compared to the eastern range supplying the material to the Bay of Bengal (Vögeli et al., 2017). The Miocene increase in primary clay mineral supply was also associated with various regional tectonic events such as the proposed breakoff of the Indian plate slab (Webb et al., 2017; Figure 5) and was accompanied by an exponential increase in the deposition of terrigenous material at the Ninety East Ridge (Figure 5e), causing a clear change in the color of the sediments (Figure S3) and, importantly, an increase in clay content (Figure 6). As all these changes were accompanied by only subtle changes in the mixture of sources being weathered they point to a shift in the weathering regime in the SAM region. A shift in the weathering regime during the mid and late Miocene cooling resulting from increased aridity and changes in the large scale atmospheric circulation in the SAM domain can reconcile much of the contrasting evidence for SAM initiation (cf. Betzler et al., 2016; Clift et al., 2008; Quade et al., 1989) but such a shift would also have wider implications for atmospheric CO_2 and global climate.

The relative reduction in secondary clay mineral formation across the Asian monsoon region would imply a decrease in the silicate weathering in the region supplying most sediments to the ocean today (Milliman & Syvitski, 1992). Although clastic sedimentation around Asia decreased from around 12 Ma to a low at 10 Ma, overall the flux was elevated since the Oligocene (Clift, 2006). Meanwhile, the Ninety East Ridge detrital mineral flux and accumulation rates on the nearby Bengal Fan increased following the global cooling (Figure 5) possibly compensating for temporary reductions elsewhere in Asia at this time (Clift, 2006). Incorporating the new results from the uniquely long and continuous record for the region obtained from the Ninety East Ridge, it seems that the total supply of sediments from Asia, and the silicate weathering of Asia may have increased during the Miocene with the potential to reduce atmospheric CO_2 concentrations. This scenario is supported by the increase in the marine Sr isotope composition (Raymo & Ruddiman, 1992) although a break in slope around the point of middle Miocene cooling (Figure 6) suggests a decrease in the supply of continental Sr. However, as the global seawater Sr isotope composition is particularly sensitive to contributions from carbonates associated with metamorphic rocks in the Lesser Himalayas (Oliver et al., 2003; Bickle et al., 2005) the research has shifted to new silicate weathering proxies such as lithium (Hathorne & James, 2006; Misra & Froelich, 2012) and beryllium isotopes (e.g., Dixon & von Blanckenburg, 2012). Using these proxies to constrain silicate weathering in a model of the geological carbon cycle suggests that to maintain the reduction in atmospheric CO_2 reconstructed for the Cenozoic while silicate weathering fluxes were constant within a few percent, the temperature (pCO_2) dependence of silicate weathering (the silicate weathering feedback) varied significantly (Caves Rugenstein et al., 2019). This hypothesized shift in the weathering regime agrees well with the observed regional changes in clay minerals and a general decrease in weathering intensity since the mid Miocene. This change is opposite to that expected from the modern system, where more secondary clays formed by silicate weathering cause river and seawater Li isotope ratios to increase (e.g., Bagard et al., 2015), as the particularly intense weathering of the middle Miocene dissolved secondary clays, thereby releasing the initially sequestered ^{6}Li (Caves Rugenstein et al., 2019). The increase of the weatherability of Miocene regolith is consistent with the relative increase in the supply of physical weathering products but the increased supply of detrital clays (Figure 6), including

secondary clays, is apparently at odds with the constant silicate weathering flux inferred from meteoric Be isotopes. A constant silicate weathering flux is also hard to reconcile with variable carbonate accumulation in the Atlantic, Pacific and Indian Ocean basins during the Miocene (e.g., Lübbers et al., 2019) and other factors related to global cooling and increased aridity such as the expansion of grasslands with thick soils (Retallack, 2001). The global sea level drop associated with Miocene global cooling may have limited the supply of alkalinity from silicate weathering reaching the oceans with more being trapped in soil carbonates. Additionally, the increase in clay supply to the Bay of Bengal and secondary clays reaching the distal Bengal fan (Figures 6d and 6g) would have increased the potential for organic carbon burial thereby potentially reducing atmospheric CO_2 (France-Lanord & Derry, 1997). Deciphering the complex interactions of monsoon climate, silicate weathering, erosion and tectonics in detail will require higher resolution records across key tectonic and climatic events. However, the data presented here strongly argue for a global shift in silicate weathering regime during the Miocene with reduced weathering intensity linked to global cooling and possibly the development of the dry winter monsoon season in Asia.

5. Conclusions

Radiogenic Sr-Nd-Pb isotope compositions of the clay-size fraction of sediments from the Bay of Bengal indicate that the clays originated from a relatively stable mixture of sources. This indicates that the spatial pattern of regional weathering, which today is strongest where monsoon rains are highest, has persisted over the last 27 Myrs. A pronounced increase in primary clay mineral abundance occurred around 13.9 Myrs ago and indicates a relative increase in physical weathering intensity around this time. This change in weathering regime was accompanied by an increased delivery of terrigenous material and clays to the core site. In combination with data obtained from cores from the east and west, a general increase in the delivery of terrigenous material to the Bay of Bengal and a regional shift in weathering regime is inferred. The timing of this shift was coincident with middle Miocene global cooling and regional tectonic reorganizations but higher resolution records will be required to distinguish between the causes. However, the emergence of the dry winter monsoon season during the Miocene would explain the regional shift in weathering regime and reconcile much of the contrasting evidence for SAM initiation at this time.

Data Availability Statement

The data presented in this study are included in the supplementary information and all new data are freely available on the PANGAEA data repository (https://doi.pangaea.de/10.1594/PANGAEA.927027).

Acknowledgments
Samples were provided by the International Ocean Discovery Program (IODP) and we thank the Kochi repository staff for their help. The hard work of all involved in IODP Exp. 353 helped to improve the age model. The authors thank Daniel Gebregiorgis for help with Figure 1, Jutta Heinze for clean lab support, Christopher Siebert for maintaining the mass spectrometer, and Rasmus Thiede, Ann Holbourn and Wolfgang Kuhnt for discussions.

References

Ahmad, S. M., Anil Babu, G., Padmakumari, V. M., Dayal, A. M., Sukhija, B. S., & Nagabhushanam, P. (2005). Sr, Nd isotopic evidence of terrigenous flux variations in the Bay of Bengal: Implications of monsoons during the last ~34,000 years. *Geophysical Research Letters*, *32*(22). https://doi.org/10.1029/2005GL024519

Ali, S., Hathorne, E. C., Frank, M., Gebregiorgis, D., Stattegger, K., Stumpf, R., et al. (2015). South Asian monsoon history over the past 60 kyr recorded by radiogenic isotopes and clay mineral assemblages in the Andaman Sea. *Geochemistry, Geophysics, Geosystems*, *16*(2), 505–521. https://doi.org/10.1002/2014GC005586

Alizai, A., Hillier, S., Clift, P. D., Giosan, L., Hurst, A., VanLaningham, S., & Macklin, M. (2012). Clay mineral variations in Holocene terrestrial sediments from the Indus Basin. *Quaternary Research*, *77*(3), 368–381. https://doi.org/10.1016/j.yqres.2012.01.008

Allen, M. B., & Armstrong, H. A. (2012). Reconciling the Intertropical Convergence Zone, Himalayan/Tibetan tectonics, and the onset of the Asian monsoon system. *Journal of Asian Earth Sciences*, *44*, 36–47. https://doi.org/10.1016/j.jseaes.2011.04.018

Awasthi, N., & Ray, J. S. (2020). The Palaeogene record of Himalayan erosion in the Andaman Basin. *Journal of Earth System Science*, *129*(1), 15. https://doi.org/10.1007/s12040-019-1266-7

Bagard, M.-L., West, A. J., Newman, K., & Basu, A. R. (2015). Lithium isotope fractionation in the Ganges–Brahmaputra floodplain and implications for groundwater impact on seawater isotopic composition. *Earth and Planetary Science Letters*, *432*, 404–414. https://doi.org/10.1016/j.epsl.2015.08.036

Betzler, C., Eberli, G. P., Kroon, D., Wright, J. D., Swart, P. K., Nath, B. N., et al. (2016). The abrupt onset of the modern South Asian Monsoon winds. *Scientific Reports*, *6*(1), 29838. https://doi.org/10.1038/srep29838

Bickle, M. J., Chapman, H. J., Bunbury, J., Harris, N. B. W., Fairchild, I. J., Ahmad, T., & Pomiès, C. (2005). Relative contributions of silicate and carbonate rocks to riverine Sr fluxes in the headwaters of the Ganges. *Geochimica et Cosmochimica Acta*, *69*(9), 2221–2240. https://doi.org/10.1016/j.gca.2004.11.019

Boos, W. R., & Kuang, Z. (2010). Dominant control of the South Asian monsoon by orographic insulation versus plateau heating. *Nature*, *463*(7278), 218–222. https://doi.org/10.1038/nature08707

Bouquillon, A., France-Lanord, C., Michard, Annie, & Tiercelin, J.-J. (1990). Sedimentology and isotopic chemistry of the Bengal fan sediments: the denudation of the Himalaya. In J. R. Cochran et al., (Eds.), Proceedings of the ocean drilling Program, 116 Scientific results. Ocean Drilling Program. https://doi.org/10.2973/odp.proc.sr.116.1990

Carter, S. C., Griffith, E. M., Clift, P. D., Scher, H. D., & Dellapenna, T. M. (2020). Clay-fraction strontium and neodymium isotopes in the Indus Fan: Implications for sediment transport and provenance. *Geological Magazine*, *157*(6), 879–894. https://doi.org/10.1017/S0016756820000394

Caves Rugenstein, J. K., Ibarra, D. E., & von Blanckenburg, F. (2019). Neogene cooling driven by land surface reactivity rather than increased weathering fluxes. *Nature*, *571*(7763), 99–102. https://doi.org/10.1038/s41586-019-1332-y

Chamley, H. (1989). *Clay sedimentology*. Berlin: Springer-Verlag. https://doi.org/10.1007/978-3-642-85916-8

Chapman, H., Bickle, M., Thaw, S. H., & Thiam, H. N. (2015). Chemical fluxes from time series sampling of the Irrawaddy and Salween Rivers, Myanmar. *Chemical Geology*, *401*, 15–27. https://doi.org/10.1016/j.chemgeo.2015.02.012

Chen, W.-H., Yan, Y., Clift, P. D., Carter, A., Huang, C.-Y., Pickering, K. T., et al. (2020). Drainage evolution and exhumation history of the eastern Himalaya: Insights from the Nicobar Fan, northeastern Indian Ocean. *Earth and Planetary Science Letters*, *548*, 116472. https://doi.org/10.1016/j.epsl.2020.116472

Clemens, S. C., Kuhnt, W., & LeVay, L. J. (2016). Expedition 353 scientists. In *Proceedings of the International Ocean Discovery Program, volume 353*. International Ocean Discovery Program. https://doi.org/10.14379/iodp.proc.353.2016

Clemens, S. C., & Oglesby, R. J. (1992). Interhemispheric moisture transport in the Indian Ocean summer monsoon: Data-model and model-model comparisons. *Paleoceanography*, *7*(5), 633–643. https://doi.org/10.1029/92PA01752

Clift, P. D. (2006). Controls on the erosion of Cenozoic Asia and the flux of clastic sediment to the ocean. *Earth and Planetary Science Letters*, *241*(3–4), 571–580. https://doi.org/10.1016/j.epsl.2005.11.028

Clift, P. D., Hodges, K. V., Heslop, D., Hannigan, R., Van Long, H., & Calves, G. (2008). Correlation of Himalayan exhumation rates and Asian monsoon intensity. *Nature Geoscience*, *1*(12), 875–880. https://doi.org/10.1038/ngeo351

Clift, P. D., & Webb, A. A. G. (2019). A history of the Asian monsoon and its interactions with solid Earth tectonics in Cenozoic South Asia. *Geological Society, London, Special Publications*, *483*(1), 631–652. https://doi.org/10.1144/SP483.1

Clift, P. D., Zhou, P., Stockli, D. F., & Blusztajn, J. (2019). Regional Pliocene exhumation of the Lesser Himalaya in the Indus drainage. *Solid Earth*, *10*(3), 647–661. https://doi.org/10.5194/se-10-647-2019

Colin, C., Turpin, L., Bertaux, J., Desprairies, A., & Kissel, C. (1999). Erosional history of the Himalayan and Burman ranges during the last two glacial–interglacial cycles. *Earth and Planetary Science Letters*, *171*(4), 647–660. https://doi.org/10.1016/S0012-821X(99)00184-3

Colleps, C. L., McKenzie, N. R., Stockli, D. F., Hughes, N. C., Singh, B. P., Webb, A. A. G., et al. (2018). Zircon (U-Th)/He thermochronometric constraints on Himalayan thrust belt exhumation, bedrock weathering, and cenozoic seawater chemistry. *Geochemistry, Geophysics, Geosystems*, *19*(1), 257–271. https://doi.org/10.1002/2017GC007191

Curray, J. R., Emmel, F. J., & Moore, D. G. (2003). The Bengal Fan: morphology, geometry, stratigraphy, history and processes. *Marine and Petroleum Geology*, *19*(10), 1191–1223. https://doi.org/10.1016/S0264-8172(03)00035-7

Damodararao, K., Singh, S. K., Rai, V. K., Ramaswamy, V., & Rao, P. S. (2016). Lithology, monsoon and sea-surface current control on provenance, dispersal and deposition of sediments over the Andaman continental shelf. *Frontiers in Marine Science*, *3*. https://doi.org/10.3389/fmars.2016.00118

Derry, L. A., & France-Lanord, C. (1996). Neogene Himalayan weathering history and river87Sr86Sr: Impact on the marine Sr record. *Earth and Planetary Science Letters*, *142*(1), 59–74. https://doi.org/10.1016/0012-821X(96)00091-X

Ding, L., Spicer, R. A., Yang, J., Xu, Q., Cai, F., Li, S., et al. (2017). Quantifying the rise of the Himalaya orogen and implications for the South Asian monsoon. *Geology*, *45*(3), 215–218. https://doi.org/10.1130/G38583.1

Dixon, J. L., & von Blanckenburg, F. (2012). Soils as pacemakers and limiters of global silicate weathering. *Comptes Rendus Geoscience*, *344*(11–12), 597–609. https://doi.org/10.1016/j.crte.2012.10.012

Fagel, N., André, L., & Debrabant, P. (1997). Multiple seawater-derived geochemical signatures in Indian oceanic pelagic clays. *Geochimica et Cosmochimica Acta*, *61*(5), 989–1008. https://doi.org/10.1016/S0016-7037(96)00392-4

Fagel, N., Debrabant, P., & André, L. (1994). Clay supplies in the Central Indian Basin since the Late Miocene: Climatic or tectonic control? *Marine Geology*, *122*(1–2), 151–172. https://doi.org/10.1016/0025-3227(94)90209-7

France-Lanord, C., Derry, L., & Michard, A. (1993). Evolution of the Himalaya since Miocene time: isotopic and sedimentological evidence from the Bengal Fan. *Geological Society, London, Special Publications*, *74*(1), 603–621. https://doi.org/10.1144/GSL.SP.1993.074.01.40

France-Lanord, C., & Derry, L. A. (1997). Organic carbon burial forcing of the carbon cycle from Himalayan erosion. *Nature*, *390*(6655), 65–67. https://doi.org/10.1038/36324

France-Lanord, C., Spiess, V., Klaus, A., & Schwenk, T. (2016). Expedition 354 Scientists. In *Proceedings of the International Ocean Discovery Program volume 354. International Ocean Discovery Program*. https://doi.org/10.14379/iodp.proc.354.2016

Frank, M. (2002). Radiogenic isotopes: Tracers of past ocean circulation and erosional input. *Reviews of Geophysics*, *40*(1), 1001. https://doi.org/10.1029/2000RG000094

Frank, M., Whiteley, N., van de Flierdt, T., Reynolds, B. C., & O'Nions, K. (2006). Nd and Pb isotope evolution of deep water masses in the eastern Indian Ocean during the past 33 Myr. *Chemical Geology*, *226*(3–4), 264–279. https://doi.org/10.1016/j.chemgeo.2005.09.024

Galy, A., & France-Lanord, C. (2001). Higher erosion rates in the Himalaya: Geochemical constraints on riverine fluxes. *Geology*, *29*(1), 23–26.

Galy, V., France-Lanord, C., Peucker-Ehrenbrink, B., & Huyghe, P. (2010). Sr–Nd–Os evidence for a stable erosion regime in the Himalaya during the past 12Myr. *Earth and Planetary Science Letters*, *290*(3–4), 474–480. https://doi.org/10.1016/j.epsl.2010.01.004

Gébelin, A., Mulch, A., Teyssier, C., Jessup, M. J., Law, R. D., & Brunel, M. (2013). The Miocene elevation of Mount Everest. *Geology*, *41*(7), 799–802. https://doi.org/10.1130/G34331.1

Gertisser, R. (2003). Trace element and Sr, Nd, Pb and O isotope variations in medium-K and high-K volcanic rocks from Merapi volcano, Central Java, Indonesia: Evidence for the involvement of subducted sediments in Sunda arc magma genesis. *Journal of Petrology*, *44*(3), 457–489. https://doi.org/10.1093/petrology/44.3.457

Giosan, L., Naing, T., Min Tun, M., Clift, P. D., Filip, F., Constantinescu, S., et al. (2018). On the Holocene evolution of the Ayeyawady megadelta. *Earth Surface Dynamics*, *6*(2), 451–466. https://doi.org/10.5194/esurf-6-451-2018

Gourlan, A. T., Meynadier, L., Allègre, C. J., Tapponnier, P., Birck, J.-L., & Joron, J.-L. (2010). Northern Hemisphere climate control of the Bengali rivers discharge during the past 4 Ma. *Quaternary Science Reviews*, *29*(19–20), 2484–2498. https://doi.org/10.1016/j.quascirev.2010.05.003

Gradstein, F. M., & Ogg, J. G. (2012). Chapter 2 - The Chronostratigraphic Scale. In F. M. Gradstein, J. G. Ogg, M. D. Schmitz, & G. M. Ogg, (Eds.), *The geologic time scale* (pp. 31–42). Boston, MA: Elsevier. https://doi.org/10.1016/B978-0-444-59425-9.00002-0

Guo, Z. T., Ruddiman, W. F., Hao, Q. Z., Wu, H. B., Qiao, Y. S., Zhu, R. X., et al. (2002). Onset of Asian Desertification by 22 Myr Ago Inferred from Loess Deposits in China, 416.
Hall, R. (2012). Late Jurassic–Cenozoic reconstructions of the Indonesian region and the Indian Ocean. *Tectonophysics*, *570–571*, 1–41. https://doi.org/10.1016/j.tecto.2012.04.021
Harlavan, Y., Erel, Y., & Blum, J. D. (2009). The coupled release of REE and Pb to the soil labile pool with time by weathering of accessory phases, Wind River Mountains, WY. *Geochimica et Cosmochimica Acta*, *73*(2), 320–336. https://doi.org/10.1016/j.gca.2008.11.002
Harris, N. (2007). Channel flow and the Himalayan–Tibetan orogen: A critical review. *Journal of the Geological Society*, *164*(3), 511–523. https://doi.org/10.1144/0016-76492006-133
Hathorne, E., & James, R. (2006). Temporal record of lithium in seawater: A tracer for silicate weathering? *Earth and Planetary Science Letters*, *246*(3–4), 393–406. https://doi.org/10.1016/j.epsl.2006.04.020
Hein, C. J., Galy, V., Galy, A., France-Lanord, C., Kudrass, H., & Schwenk, T. (2017). Post-glacial climate forcing of surface processes in the Ganges–Brahmaputra river basin and implications for carbon sequestration. *Earth and Planetary Science Letters*, *478*, 89–101. https://doi.org/10.1016/j.epsl.2017.08.013
Hemming, S. R., & McLennan, S. M. (2001). Pb isotope compositions of modern deep sea turbidites. *Earth and Planetary Science Letters*, *184*(2), 489–503. https://doi.org/10.1016/S0012-821X(00)00340-X
Heroy, D. C., Kuehl, S. A., & Goodbred, S. L. (2003). Mineralogy of the Ganges and Brahmaputra Rivers: implications for river switching and Late Quaternary climate change. *Sedimentary Geology*, *155*(3–4), 343–359. https://doi.org/10.1016/S0037-0738(02)00186-0
Holbourn, A. E., Kuhnt, W., Clemens, S. C., Kochhann, K. G. D., Jöhnck, J., Lübbers, J., & Andersen, N. (2018). Late Miocene climate cooling and intensification of southeast Asian winter monsoon. *Nature Communications*, *9*(1), 1584. https://doi.org/10.1038/s41467-018-03950-1
Hovan, A., & Rea, K. (1992). Southern African aridity and sediment delivery from the Himalayas. *Paleoceanography*, *7*, 833–860.
Iaffaldano, G., Husson, L., & Bunge, H.-P. (2011). Monsoon speeds up Indian plate motion. *Earth and Planetary Science Letters*, *304*(3–4), 503–510. https://doi.org/10.1016/j.epsl.2011.02.026
Joussain, R., Colin, C., Liu, Z., Meynadier, L., Fournier, L., Fauquembergue, K., et al. (2016). Climatic control of sediment transport from the Himalayas to the proximal NE Bengal Fan during the last glacial-interglacial cycle. *Quaternary Science Reviews*, *148*, 1–16. https://doi.org/10.1016/j.quascirev.2016.06.016
Krishna, K. S., Ismaiel, M., Srinivas, K., Rao, D. G., Mishra, J., & Saha, D. (2016). Sediment pathways and emergence of Himalayan source material in the Bay of Bengal. *Current Science*, *110*(3), 10.
Kumar, V. S., Pathak, K. C., Pednekar, P., Raju, N. S. N., & Gowthaman, R. (2006). Coastal processes along the Indian coastline. *Current Science*, *91*(4), 8.
Li, G., Chen, J., Ji, J., Liu, L., Yang, J., & Sheng, X. (2007). Global cooling forced increase in marine strontium isotopic ratios: Importance of mica weathering and a kinetic approach. *Earth and Planetary Science Letters*, *254*(3–4), 303–312. https://doi.org/10.1016/j.epsl.2006.11.045
Li, J., Liu, S., Shi, X., Feng, X., Fang, X., Cao, P., et al. (2017). Distributions of clay minerals in surface sediments of the middle Bay of Bengal: Source and transport pattern. *Continental Shelf Research*, *145*, 59–67. https://doi.org/10.1016/j.csr.2017.06.017
Li, Y., Clift, P. D., Murray, R. W., Exnicios, E., Ireland, T., & Böning, P. (2019). Asian summer monsoon influence on chemical weathering and sediment provenance determined by clay mineral analysis from the Indus Submarine Canyon. *Quaternary Research*, *93*, 23–39. https://doi.org/10.1017/qua.2019.44
Licht, A., France-Lanord, C., Reisberg, L., Fontaine, C., Soe, A. N., & Jaeger, J.-J. (2013). A palaeo Tibet–Myanmar connection? Reconstructing the Late Eocene drainage system of central Myanmar using a multi-proxy approach. *Journal of the Geological Society*, *170*(6), 929–939. https://doi.org/10.1144/jgs2012-126
Licht, A., van Cappelle, M., Abels, H. A., Ladant, J.-B., Trabucho-Alexandre, J., France-Lanord, C., et al. (2014). Asian monsoons in a late Eocene greenhouse world. *Nature*, *513*(7519), 501–506. https://doi.org/10.1038/nature13704
Lightfoot, P. C., Hawkesworth, C. J., Devey, C. W., Rogers, N. W., & Calsteren, P. W. C. V. (1990). Source and Differentiation of Deccan Trap Lavas: Implications of Geochemical and Mineral Chemical Variations. *Journal of Petrology*, *31*(5), 1165–1200. https://doi.org/10.1093/petrology/31.5.1165
Lübbers, J., Kuhnt, W., Holbourn, A. E., Bolton, C. T., Gray, E., Usui, Y., et al. (2019). The Middle to Late Miocene "Carbonate Crash" in the Equatorial Indian Ocean. *Paleoceanography and Paleoclimatology*, 2018PA003482. *34*, https://doi.org/10.1029/2018PA003482
Lupker, M., France-Lanord, C., Lavé, J., Bouchez, J., Galy, V., Métivier, F., et al. (2011). A Rouse-based method to integrate the chemical composition of river sediments: Application to the Ganga basin. *Journal of Geophysical Research*, *116*(F4), F04012. https://doi.org/10.1029/2010JF001947
McArthur, J. M., Howarth, R. J., & Bailey, T. R. (2001). Strontium isotope stratigraphy: Lowess version 3: Best fit to the marine Sr-isotope curve for 0–509 Ma and accompanying look-up table for deriving numerical age. *The Journal of Geology*, *109*(2), 155–170. https://doi.org/10.1086/319243
McNeill, L. C., Dugan, B., Backman, J., Pickering, K. T., Pouderoux, H. F. A., Henstock, T. J., et al. (2017). Understanding Himalayan erosion and the significance of the Nicobar Fan. *Earth and Planetary Science Letters*, *475*, 134–142. https://doi.org/10.1016/j.epsl.2017.07.019
Michalopoulos, P., & AIIer, R. C. (1995). Rapid clay mineral formation in Amazon Delta sediments. *Reverse Weathering and Oceanic Elemental Cycles*, *270*, 5.
Milligan, T. G., & Hill, P. S. (1998). A laboratory assessment of the relative importance of turbulence, particle composition, and concentration in limiting maximal floc size and settling behaviour. *Journal of Sea Research*, *39*(3–4), 227–241. https://doi.org/10.1016/S1385-1101(97)00062-2
Milliman, J. D., & Syvitski, J. P. M. (1992). Geomorphic/tectonic control of sediment discharge to the ocean: The importance of small mountainous rivers. *The Journal of Geology*, *100*(5), 525–544. https://doi.org/10.1086/629606
Misra, S., & Froelich, P. N. (2012). Lithium isotope history of cenozoic seawater: Changes in silicate weathering and reverse weathering. *Science*, *335*(6070), 818–823. https://doi.org/10.1126/science.1214697
Molnar, P., England, P., & Martinod, J. (1993). Mantle dynamics, uplift of the Tibetan plateau, and the Indian monsoon. *Reviews of Geophysics*, *31*(4), 357. https://doi.org/10.1029/93RG02030
Nagender Nath, B., Makishima, A., Noordmann, J., Tanaka, R., & Nakamura, E. (2009). Comprehensive analysis for major, minor and trace element contents and Sr-Nd-Pb-Hf isotope ratios in sediment reference materials, JSd-1 and MAG-1. *Geochemical Journal*, *43*(3), 207–216. https://doi.org/10.2343/geochemj.1.0018
Najman, Y., Bickle, M., BouDagher-Fadel, M., Carter, A., Garzanti, E., Paul, M., et al. (2008). The Paleogene record of Himalayan erosion: Bengal Basin, Bangladesh. *Earth and Planetary Science Letters*, *273*(1–2), 1–14. https://doi.org/10.1016/j.epsl.2008.04.028

Najman, Y., Mark, C., Barfod, D. N., Carter, A., Parrish, R., Chew, D., & Gemignani, L. (2019). Spatial and temporal trends in exhumation of the Eastern Himalaya and syntaxis as determined from a multitechnique detrital thermochronological study of the Bengal Fan. *GSA Bulletin*, *131*(9–10), 1607–1622. https://doi.org/10.1130/B35031.1

Najman, Y., Sobel, E. R., Millar, I., Stockli, D. F., Govin, G., Lisker, F., et al. (2020). The exhumation of the Indo-Burman Ranges, Myanmar. *Earth and Planetary Science Letters*, *530*, 115948. https://doi.org/10.1016/j.epsl.2019.115948

Oliver, L., Harris, N., Bickle, M., Chapman, H., Dise, N., & Horstwood, M. (2003). Silicate weathering rates decoupled from the 87Sr/86Sr ratio of the dissolved load during Himalayan erosion. *Chemical Geology*, *201*(1–2), 119–139. https://doi.org/10.1016/S0009-2541(03)00236-5

Peirce, J., Weissel, J., & Shipboard Scientific Party. (1989). *Site 758 Proc. ODP*. College Station, TX: Ocean Drilling Program.

Quade, J., Cerling, T. E., & Bowman, J. R. (1989). Development of Asian monsoon revealed by marked ecological shift during the latest Miocene in northern Pakistan. *Nature*, *342*(6246), 163–166. https://doi.org/10.1038/342163a0

Raymo, M. E., & Ruddiman, W. F. (1992). Tectonic forcing of late Cenozoic climate. *Nature*, *359*(6391), 117–122. https://doi.org/10.1038/359117a0

Retallack, G. J. (2001). Cenozoic expansion of grasslands and climatic cooling. *The Journal of Geology*, *109*(4), 407–426. https://doi.org/10.1086/320791

Robinson, R. A. J., Bird, M. I., Oo, N. W., Hoey, T. B., Aye, M. M., Higgitt, D. L., et al. (2007). The Irrawaddy river sediment flux to the Indian Ocean: The original nineteenth-century data revisited. *The Journal of Geology*, *115*(6), 629–640. https://doi.org/10.1086/521607

Shen, X., Wan, S., France-Lanord, C., Clift, P. D., Tada, R., Révillon, S., et al. (2017). History of Asian eolian input to the Sea of Japan since 15 Ma: Links to Tibetan uplift or global cooling? *Earth and Planetary Science Letters*, *474*, 296–308. https://doi.org/10.1016/j.epsl.2017.06.053

Singh, S. K., & France-Lanord, C. (2002). Tracing the distribution of erosion in the Brahmaputra watershed from isotopic compositions of stream sediments. *Earth and Planetary Science Letters*, *202*(3–4), 645–662. https://doi.org/10.1016/S0012-821X(02)00822-1

Srinivas, B., & Sarin, M. M. (2013). Atmospheric dry-deposition of mineral dust and anthropogenic trace metals to the Bay of Bengal. *Journal of Marine Systems*, *126*, 56–68. https://doi.org/10.1016/j.jmarsys.2012.11.004

Steinke, S., Groeneveld, J., Johnstone, H., & Rendle-Bühring, R. (2010). East Asian summer monsoon weakening after 7.5 Ma: Evidence from combined planktonic foraminifera Mg/Ca and δ18O (ODP Site 1146; northern South China Sea). *Palaeogeography, Palaeoclimatology, Palaeoecology*, *289*(1–4), 33–43. https://doi.org/10.1016/j.palaeo.2010.02.007

Tanaka, T., Togashi, S., Kamioka, H., Amakawa, H., Kagami, H., Hamamoto, T., et al. (2000). JNdi-1: a neodymium isotopic reference in consistency with LaJolla neodymium. *Chemical Geology*, *168*(3–4), 279–281. https://doi.org/10.1016/S0009-2541(00)00198-4

Thiede, R. C., Bookhagen, B., Arrowsmith, J. R., Sobel, E. R., & Strecker, M. R. (2004). Climatic control on rapid exhumation along the Southern Himalayan Front. *Earth and Planetary Science Letters*, *222*(3–4), 791–806. https://doi.org/10.1016/j.epsl.2004.03.015

Thiry, M. (2000). Palaeoclimatic interpretation of clay minerals in marine deposits: an outlook from the continental origin. *Earth-Science Reviews*, *49*(1–4), 201–221. https://doi.org/10.1016/S0012-8252(99)00054-9

Tripathi, J. K., Bock, B., & Rajamani, V. (2013). Nd and Sr isotope characteristics of quaternary Indo-Gangetic plain sediments: Source distinctiveness in different geographic regions and its geological significance. *Chemical Geology*, *344*, 12–22. https://doi.org/10.1016/j.chemgeo.2013.02.016

Unger, D., Ittekkot, V., Schäfer, P., Tiemann, J., & Reschke, S. (2003). Seasonality and interannual variability of particle fluxes to the deep Bay of Bengal: influence of riverine input and oceanographic processes. *Deep Sea Research Part II: Topical Studies in Oceanography*, *50*(5), 897–923. https://doi.org/10.1016/S0967-0645(02)00612-4

Violette, A., Goddéris, Y., Maréchal, J.-C., Riotte, J., Oliva, P., Kumar, M. S. M., et al. (2010). Modelling the chemical weathering fluxes at the watershed scale in the Tropics (Mule Hole, South India): Relative contribution of the smectite/kaolinite assemblage versus primary minerals. *Chemical Geology*, *277*(1–2), 42–60. https://doi.org/10.1016/j.chemgeo.2010.07.009

Vögeli, N., Najman, Y., van der Beek, P., Huyghe, P., Wynn, P. M., Govin, G., et al. (2017). Lateral variations in vegetation in the Himalaya since the Miocene and implications for climate evolution. *Earth and Planetary Science Letters*, *471*, 1–9. https://doi.org/10.1016/j.epsl.2017.04.037

Wan, S., Li, A., Clift, P. D., & Stuut, J.-B. W. (2007). Development of the East Asian monsoon: Mineralogical and sedimentologic records in the northern South China Sea since 20 Ma. *Palaeogeography, Palaeoclimatology, Palaeoecology*, *254*(3–4), 561–582. https://doi.org/10.1016/j.palaeo.2007.07.009

Wang, C., Dai, J., Zhao, X., Li, Y., Graham, S. A., He, D., et al. (2014). Outward-growth of the Tibetan Plateau during the Cenozoic: A review. *Tectonophysics*, *621*, 1–43. https://doi.org/10.1016/j.tecto.2014.01.036

Webb, A. A. G., Guo, H., Clift, P. D., Husson, L., Müller, T., Costantino, D., et al. (2017). The Himalaya in 3D: Slab dynamics controlled mountain building and monsoon intensification. *Lithosphere*, *1*, L636. https://doi.org/10.1130/L636.1

Zachos, J. C., Dickens, G. R., & Zeebe, R. E. (2008). An early Cenozoic perspective on greenhouse warming and carbon-cycle dynamics. *Nature*, *451*(7176), 279–283. https://doi.org/10.1038/nature06588

Zahirovic, S., Flament, N., Dietmar Müller, R., Seton, M., & Gurnis, M. (2016). Large fluctuations of shallow seas in low-lying Southeast Asia driven by mantle flow. *Geochemistry, Geophysics, Geosystems*, *17*(9), 3589–3607. https://doi.org/10.1002/2016GC006434

Zhao, H. (2004). On the relationship between Tibetan snow cover, the Tibetan plateau monsoon and the Indian summer monsoon. *Geophysical Research Letters*, *31*(14), L14204. https://doi.org/10.1029/2004GL020040

References From the Supporting Information

Ahmad, S. M., Padmakumari, V. M., & Babu, G. A. (2009). Strontium and neodymium isotopic compositions in sediments from Godavari, Krishna and Pennar rivers. *Current Science*, *97*(12), 1766–1769.

Ali, S., Hathorne, E. C., & Frank, M. (2021). *Radiogenic Sr, Nd and Pb isotope data and clay mineral abundances of the < 2 µm size fraction of ODP Hole 121-758A*. PANGAEA. https://doi.pangaea.de/10.1594/PANGAEA.927027

Allen, R., Najman, Y., Carter, A., Barfod, D., Bickle, M. J., Chapman, H. J., et al. (2008). Provenance of the Tertiary sedimentary rocks of the Indo-Burman Ranges, Burma (Myanmar): Burman arc or Himalayan-derived? *Journal of the Geological Society*, *165*(6), 1045–1057. https://doi.org/10.1144/0016-76492007-143

Banerjee, B., Masood Ahmad, S., Babu, E. V. S. S. K., Padmakumari, V. M., Kumar Beja, S., Satyanarayanan, M., & Keshav Krishna, A. (2019). Geochemistry and isotopic study of southern Bay of Bengal sediments: Implications for provenance and paleoenvironment during the middle Miocene. *Palaeogeography, Palaeoclimatology, Palaeoecology*, *514*, 156–167. https://doi.org/10.1016/j.palaeo.2018.10.022

Blott, S. J., & Pye, K. (2001). GRADISTAT: a grain size distribution and statistics package for the analysis of unconsolidated sediments. *Earth Surface Processes and Landforms*, *26*(11), 1237–1248. https://doi.org/10.1002/esp.261

Chester, R., & Hughes, M. J. (1967). A chemical technique for the separation of ferro-manganese minerals, carbonate minerals and adsorbed trace elements from pelagic sediments. *Chemical Geology*, *14*, 249–262.

Dehn, J., Farrell, J. W., Weissel, J., Peirce, J., Taylor, E., Alt, J., et al. (1991). Neogene tephrochronology from site 758 on northern Ninety east Ridge: Indonesian arc volcanism of the past 5 MA. In Proceedings of the Ocean Drilling Program. Scientific Results.

Ehlert, C., Frank, M., Haley, B. A., Böniger, U., De Deckker, P., & Gingele, F. X. (2011). Current transport versus continental inputs in the eastern Indian Ocean: Radiogenic isotope signatures of clay size sediments. *Geochemistry, Geophysics, Geosystems*, *12*(6). https://doi.org/10.1029/2011GC003544

Galy, A., France-Lanord, C., & Derry, L. A. (1996). The late oligocene-early miocene Himalayan belt constraints deduced from isotopic compositions of early miocene turbidites in the Bengal fan. *Tectonophysics*, *260*(1–3), 109–118. https://doi.org/10.1016/0040-1951(96)00079-0

Garçon, M., & Chauvel, C. (2014). Where is basalt in river sediments, and why does it matter? *Earth and Planetary Science Letters*, *407*, 61–69. https://doi.org/10.1016/j.epsl.2014.09.033

Garçon, M., Chauvel, C., France-Lanord, C., Huyghe, P., & Lavé, J. (2013). Continental sedimentary processes decouple Nd and Hf isotopes. *Geochimica et Cosmochimica Acta*, *121*, 177–195. https://doi.org/10.1016/j.gca.2013.07.027

Garçon, M., Chauvel, C., France-Lanord, C., Limonta, M., & Garzanti, E. (2013). Removing the "heavy mineral effect" to obtain a new Pb isotopic value for the upper crust. *Geochemistry, Geophysics, Geosystems*, *14*(9), 3324–3333. https://doi.org/10.1002/ggge.20219

Gasparon, M. (1993). *Origin and evolution of mafic volcanics of Sumatra (Indonesia): Their mantle sources, and the roles of subducted oceanic sediments and crustral contamination*. PhD Thesis. University of Tasmania.

Helios Rybicka, E., & Calmano, W. (1988). Changes in physico-chemical properties of some clay minerals by reducing extraction reagents. *Applied Clay Science*, *3*(1), 75–84. https://doi.org/10.1016/0169-1317(88)90007-5

Hillier, S. (1999). Quantitative Analysis of Clay and other Minerals in Sandstones by X-Ray Powder Diffraction (XRPD). In R. H. Worden, & S. Morad, (Eds)., *Clay mineral cements in sandstones* (pp. 213–251). Oxford, UK: Blackwell Publishing Ltd. https://doi.org/10.1002/9781444304336.ch11

Jacobsen, S. B., & Wasserburg, G. J. (1980). Sm-Nd isotopic evolution of chondrites. *Earth and Planetary Science Letters*, *50*(1), 139–155. https://doi.org/10.1016/0012-821X(80)90125-9

Lee, J., Kim, S., Lee, J. I., Cho, H. G., Phillips, S. C., & Khim, B.-K. (2020). Monsoon-influenced variation of clay mineral compositions and detrital Nd-Sr isotopes in the western Andaman Sea (IODP Site U1447) since the late Miocene. *Palaeogeography, Palaeoclimatology, Palaeoecology*, *538*, 109339. https://doi.org/10.1016/j.palaeo.2019.109339

Lightfoot, P., & Hawkesworth, C. (1988). Origin of Deccan Trap lavas: evidence from combined trace element and Sr-, Nd- and Pb-isotope studies. *Earth and Planetary Science Letters*, *91*(1–2), 89–104. https://doi.org/10.1016/0012-821X(88)90153-7

Mahoney, J., Macdougall, J., Lugmair, G., Murali, A., Sankardas, M., & Gopalan, K. (1982). Origin of the Deccan trap flows at Mahabaleshwar inferred from Nd and Sr isotopic and chemical evidence. *Earth and Planetary Science Letters*, *60*(1), 47–60. https://doi.org/10.1016/0012-821X(82)90019-X

Millot, R., Allègre, C.-J., Gaillardet, J., & Roy, S. (2004). Lead isotopic systematics of major river sediments: a new estimate of the Pb isotopic composition of the upper continental crust. *Chemical Geology*, *203*(1–2), 75–90. https://doi.org/10.1016/j.chemgeo.2003.09.002

Ottner, F., Gier, S., Kuderna, M., & Schwaighofer, B. (2000). Results of an inter-laboratory comparison of methods for quantitative clay analysis. *Applied Clay Science*, *17*(5–6), 223–243. https://doi.org/10.1016/S0169-1317(00)00015-6

Phillips, S. C. (2014). Long-timescale variation in bulk and clay mineral composition of Indian continental margin sediments in the Bay of Bengal, Arabian Sea, and Andaman Sea. *Marine and Petroleum Geology*, *58*(Part A), 117–138.

Simon, M. H., Babin, D. P., Goldstein, S. L., Cai, M. Y., Liu, T., Han, X., et al. (2020). Development of a protocol to obtain the composition of terrigenous detritus in marine sediments -a pilot study from International Ocean Discovery Program Expedition 361. *Chemical Geology*, *535*, 119449. https://doi.org/10.1016/j.chemgeo.2019.119449

Trentesaux, A., Recourt, P., Bout-Roumazeilles, V., & Tribovillard, N. (2001). Carbonate grain-size distribution in hemipelagic sediments from a laser particle sizer. *Journal of Sedimentary Research*, *71*(5), 858–862. https://doi.org/10.1306/2DC4096E-0E47-11D7-8643000102C1865D

Turner, S., & Foden, J. (2001). U, Th and Ra disequilibria, Sr, Nd and Pb isotope and trace element variations in Sunda arc lavas: Predominance of a subducted sediment component. *Contributions to Mineralogy and Petrology*, *142*(1), 43–57. https://doi.org/10.1007/s004100100271

Vlastélic, I., Abouchami, W., Galer, S. J. G., & Hofmann, A. W. (2001). Geographic control on Pb isotope distribution and sources in Indian Ocean Fe-Mn deposits. *Geochimica et Cosmochimica Acta*, *65*(23), 4303–4319. https://doi.org/10.1016/S0016-7037(01)00713-X

Wilkens, R. H., Westerhold, T., Drury, A. J., Lyle, M., Gorgas, T., & Tian, J. (2017). Revisiting the Ceara Rise, equatorial Atlantic Ocean: isotope stratigraphy of ODP Leg 154 from 0 to 5 Ma. *Climate of the Past*, *13*(7), 779–793. https://doi.org/10.5194/cp-13-779-2017

Wilson, D. J., Galy, A., Piotrowski, A. M., & Banakar, V. K. (2015). Quaternary climate modulation of Pb isotopes in the deep Indian Ocean linked to the Himalayan chemical weathering. *Earth and Planetary Science Letters*, *424*, 256–268. https://doi.org/10.1016/j.epsl.2015.05.014